Translational energy dependence of $O^+(^4S)+N_2 \rightarrow NO^+ + N$ from thermal energies to 30 eV c.m.

J. D. Burley, Kent M. Ervin, and P. B. Armentrout[a)]
Department of Chemistry, University of California, Berkeley, California 94720

(Received 6 October 1986; accepted 10 November 1986)

Guided ion beam mass spectrometry is used to examine the kinetic energy dependence of the reaction of ground state atomic oxygen ion with molecular nitrogen. An $O^+(^4S)$ source which produces less than 0.06% excited states is described. Cross sections for the $NO^+ + N$ product channel decrease with increasing energy below 0.25 eV but increase with energy at higher energies. Analysis of the region above 0.25 eV finds an effective barrier of 0.33 ± 0.08 eV which previous theoretical work suggests is on the $N_2O^+(1\,^4A'')$ hypersurface. Below this barrier, ground state products can only be formed via a spin-forbidden surface transition. The magnitude and energy dependence of the probability for this transition are in reasonable agreement with a Landau–Zener formalism. These results are compared to previous ion beam, flowing afterglow (FA), and flow/drift tube (FD) studies. Apparent disagreement between the present data and previous FA and FD measurement is shown to be caused primarily by differences in the ion energy distributions.

INTRODUCTION

It was long thought that exothermic ion–molecule reactions proceed efficiently with cross sections that decline as predicted by the Langevin–Gioumousis–Stevenson (LGS) model,[1]

$$\sigma_L(E) = \pi e(2\alpha/E)^{1/2}, \tag{1}$$

where E is the interaction energy of the reactants, e is the electronic charge, and α is the polarizability of the target molecule. One system which was found to contradict this predicted behavior is reaction (2), exothermic by 1.08 eV. This process,

$$O^+(^4S) + N_2(X\,^1\Sigma_g^+) \rightarrow NO^+(X\,^1\Sigma^+) + N(^4S), \tag{2}$$

is extremely important in understanding the chemistry of the upper atmosphere and its atypical energy dependence is also of fundamental interest. For these reasons, reaction (2) is one of the better studies ion–molecule reactions. Ion beam,[2–10] flow/drift tube (FD),[11–14] selected ion flow tube (SIFT),[15,16] and flowing afterglow (FA) studies[17–23] have yielded information on the behavior of this reaction from thermal energies to over 20 eV.

While the collective energy range of these experiments is broad, the ability of any one study to examine the kinetic energy dependence over a wide range has been limited. Typically, ion beam studies have been useful for examining relatively high energy regimes but have been unable to generate reliable data below ~ 1 eV. FA methods provide access to the lowest energy regions, but are incapable of going much above 600 K ($3k_BT/2 = 0.078$ eV). Recent FD results bridge the gap between ion beam and FA studies, but do not extend to more than 3 eV. Unfortunately, the ion energy distributions in FD methods are relatively broad and uncertain at energies above a few tenths of an eV. Despite this, a very careful and detailed analysis of the FD results has provided the cross section for reaction (2) over a two order-of-magnitude energy range.[13] The cross section obtained from this analysis disagrees somewhat with the results of beam studies above 1 eV but reproduces the rate constant behavior in both He and Ar buffers.[13] Overall, the consensus of all these studies is that the behavior of reaction (2) shows an inefficient channel at very low energies, < 0.2 eV, followed by a sharp increase in the cross section at higher energies.

To understand this behavior, theoretical work involving the use of potential energy surface correlation diagrams[24–32] and phase space calculations[33] has been carried out. These studies conclude that the failure of reaction (2) to proceed efficiently is due to a barrier on the surface which adiabatically correlates ground state reactants and products. In $C_{\infty v}$ symmetry, this is a $^4\Sigma^-$ surface which corresponds to an excited state of N_2O^+. If the angle of approach is altered, the barrier on this surface (now $1\,^4A''$) is lower with a calculated minimum of 0.15 ± 0.1 eV at a NNO angle of 126°.[28] This surface is shown schematically in Fig. 1. At the lowest kinetic energies, reaction can only occur via a spin-forbidden transition between this $N_2O^+(1\,^4A'')$ surface and the $N_2O^+(1\,^2A'')$ surface. Hopper[28] has proposed two possible mechanisms for this low energy process: either the collisionally stabilized multistep reaction,

$$O^+(^4S) + N_2 + M \rightarrow N_2\text{–}O^+(1\,^4A'') + M, \tag{3a}$$

$$N_2\text{–}O^+(1\,^4A'') \rightarrow N_2O^+(1\,^2A''), \tag{3b}$$

$$N_2O^+(1\,^2A'') \rightarrow NO^+ + N, \tag{3c}$$

or the single collision reaction,

$$O^+(^4S) + N_2 \rightarrow N_2O^+(1\,^2A'') \rightarrow NO^+ + N. \tag{4}$$

Hopper has argued that reaction (3) is the primary mechanism for reaction (2) at low energies and that reaction (4) is unimportant until energies below 0.001 eV. The rationale behind this assumption is that collisional stabilization of the

[a)] NSF Presidential Young Investigator 1984–89; Alfred P. Sloan Fellow.

 0021-9606/87/041944-10$02.10

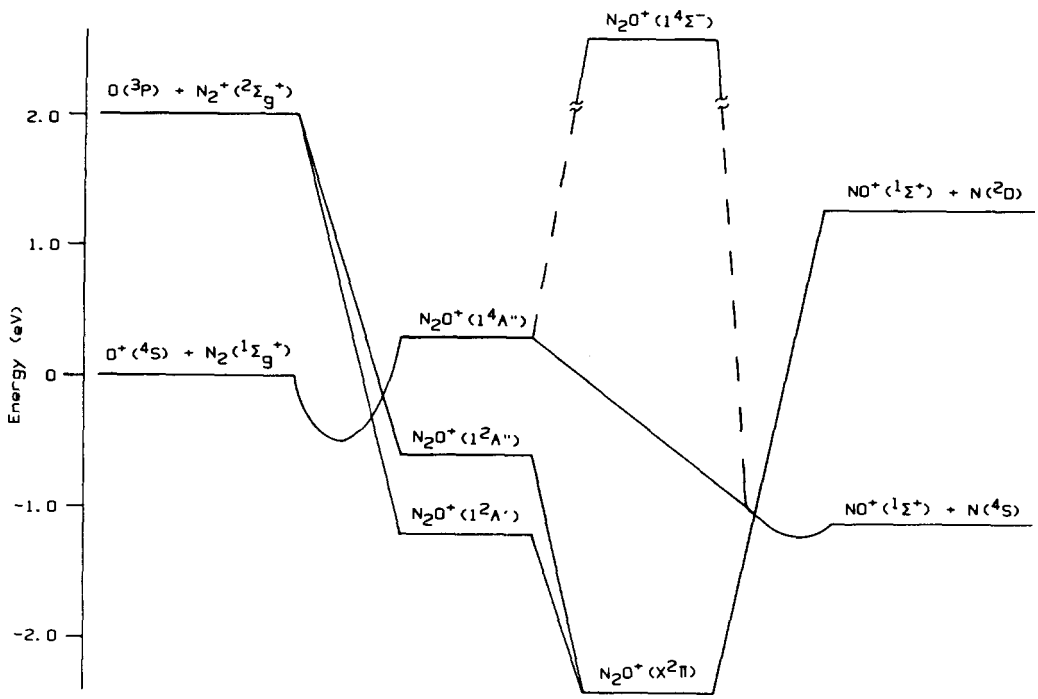

FIG. 1. Electronic state correlation diagram for N_2O^+ in C_S (130°) and $C_{\infty v}$ symmetry. The energies of the C_S intermediates, the location of the crossing between the $1\,^4A''$ and $1\,^2A''$ surfaces, and the depths of the $O^+ + N_2$ and $NO^+ + N$ ion-induced dipole potential wells are taken from Hopper, Ref. 28.

$N_2O^+(1\,^4A'')$ intermediate in step (3a) enhances step (3b) by allowing for multiple "passes" of the N_2O^+ system through the intersection of the $1\,^4A''$ and $1\,^2A''$ surfaces. This proposal has not been subjected to an experimental test since all studies of reaction (2) at low energies[11–23] have been performed in flow tubes where a rare gas buffer is available as the third body in step (3a).

One of the experimental problems associated with studies of reaction (2) is the production of pure ground state $O^+(^4S)$. This is a particular problem since the metastable excited states [$O^+(^2D)$ and $O^+(^2P)$, 3.3 and 5.0 eV above the ground state, respectively] are very reactive with N_2.[34] While charge transfer from ground state $O^+(^4S)$, reaction (5), is endothermic by 1.96 eV, charge transfer from $O^+(^2D)$, reaction (6), and from $O^+(^2P)$, reaction (7), are quite efficient.[34] If it is assumed that the

$$O^+(^4S) + N_2 \rightarrow N_2^+(X\,^2\Sigma_g^+) + O(^3P), \quad (5)$$

$$O^+(^2D) + N_2 \rightarrow N_2^+ + O(^3P), \quad (6)$$

$$O^+(^2P) + N_2 \rightarrow N_2^+ + O(^3P), \quad (7)$$

excited state charge transfer reactions produce $N_2^+(X\,^2\Sigma_g^+)$, the ground electronic state, then reactions (6) and (7) are exothermic by 1.36 and 3.06 eV, respectively. If the first excited state, $N_2^+(A\,^2\pi_u)$, is produced, then the respective exothermicities are 0.20 and 1.90 eV. Collisional quenching of $O^+(^2P)$, reaction (8) is also very efficient[34]:

$$O^+(^2P) + N_2 \rightarrow O^+(^4S) + N_2 \quad (8)$$

However, experiments by Rutherford and Vroom[5] show that neither $O^+(^2D)$ nor $O^+(^2P)$ reacts with N_2 to produce NO^+ to any appreciable extent.[35]

In the present study, guided ion beam mass spectrometry is used to investigate the kinetic energy dependence of reaction (2) from 0.03 to 30.0 eV. A source which provides beams of $O^+(^4S)$ with less than 0.06% excited states is described. The results are compared to those discussed in the literature.[2–23] and the observed behavior is interpreted in light of the theoretical calculations.[27–32] Several points are of particular interest. Can the guided ion beam technique provide accurate information at the very low kinetic energies previously available to only flowing afterglow and flow/drift methods? If so, is the cross section derived from FD rate constant data accurate? Since the beam technique is performed without the presence of a buffer gas, which mechanism, (3) or (4), is dominant at the lowest kinetic energies?

EXPERIMENTAL

General

The apparatus used in these investigations has been described in detail elsewhere.[36] Ground state O^+ is produced in a source discussed below. The ions are extracted from the source, focused by a series of electrostatic lenses, and accelerated for mass analysis in a magnetic momentum analyzer. After mass selection, the ion beam is decelerated to the desired kinetic energy and focused into an octopole ion beam guide. This device uses rf fields to create a potential well in the radial direction without altering the axial motion of the ions. The octopole guides the ion beam through an interaction region containing the reactant gas. Use of the octopole insures that both reactant and product ions are efficiently collected. All trapped ions are extracted from the octopole,

focused into a quadrupole mass filter for mass analysis, and then detected by a Daly type[37] secondary electron scintillation detector. A DEC MINC computer controls the apparatus and automates data acquisition. Raw ion intensities are converted to absolute reaction cross sections as described previously.[36] These cross sections are corrected for random counting noise and for reaction which occurs outside the gas cell. Overall, we estimate the absolute magnitude of our cross section measurements to be accurate to $\pm$ 20%.

Reactant gas pressures within the interaction region are measured with a capacitance manometer, and are, typically within the range of 0.02–0.10 mTorr. This is sufficiently low that secondary ion–molecule collisions are highly unlikely, although not of zero probability.[38] Careful measurements of the pressure dependence establish that the cross sections reported here are independent of pressure, as expected for processes due to a single ion–molecule collision.

To determine the absolute zero and distribution of the ion energy, a retarding field anlaysis is used in which the dc potential of the interaction region is swept through the nominal ion energy zero. Since the interaction region and the energy analysis region are physically the same, this method avoids ambiguities resulting from space charge effects, contact potentials, and focusing aberrations. The derivative of the retarding field analysis curve is very close to a Gaussian distribution. The true ion beam energy zero is taken as the peak of this distribution, and can be determined to a precision of $\pm$ 0.01 eV lab, as can the corresponding full width at half-maximum (FWHM). For this study, a typical FWHM is 0.3 eV in the laboratory frame. At the very low energies in the fall-off region of the retarding analysis curve, the slower ions are truncated from the distribution. This produces a narrowing of the ion energy distribution at these low energies. We take advantage of this effect to extend the energy range for cross section measurements to below one FWHM of the beam energy spread. This procedure has been described in detail elsewhere.[36] Unless stated otherwise, all energies quoted in this report correspond to the center-of-mass interaction energy E_0, which is related to the laboratory energy of the ion by Eq. (9), where M is the mass of the target nitrogen molecule and m is the mass of the incident O^+ ion,

$$E_0 = E_{\text{lab}} \cdot M/(m+M). \tag{9}$$

Ion source

Atomic oxygen ions are produced by electron impact (EI) ionization of CO_2 at electron energies (Ee) of 70–100 eV. According to Hughes and Tiernan,[6] a beam of O^+ produced from CO_2 at Ee = 60 eV consists of approximately 96% ground state (^4S) and 4% excited states (^2D and higher). At the higher Ee's used in these experiments, the fraction of excited state O^+ initially present in the beam could be somewhat larger. If molecular oxygen is used as the source gas in place of CO_2, then the percentage of excited state O^+ produced by 60 eV EI rises to 28%.[3,6] This makes O_2 a less attractive source gas for production of $O^+(^4S)$ than CO_2; however, we use it as the source gas for experiments which test the effectiveness of the state selection process described below.

To remove the excited state ions produced by EI, the O^+ beam is injected into a high pressure drift cell containing molecular nitrogen as a bath gas. The drift cell is similar in design to the one described by Bowers and co-workers[39] and has been described in detail in a previous report.[40] In the drift cell, the ions undergo multiple collisions with the bath gas while under the influence of a weak electric field. The approximate residence time of the ions in the drift cell is given by Eq. (10),

$$\tau = Z/KE, \tag{10}$$

where K is the ion mobility in cm^2/Vs, Z is the drift distance (2 cm), and E is the electric field strength (2.5 V/cm). The ion mobility can be calculated from Eq. (11),

$$K = K_0(760/P)(T/273.16), \tag{11}$$

where K_0 is the reduced mobility, P is the pressure of the bath gas in Torr, and T is the temperature of the gas (300 K). Although the reduced mobility of O^+ in nitrogen has not been measured directly, the reduced mobilities for ions similar in mass to oxygen range from 2–3 cm^2/Vs.[41] At a pressure of 0.150 Torr, this corresponds to τ = 50–70 μs. The average number of collisions experienced by an ion traversing the cell can be obtained by multiplying the residence time of the ion by the rate constant for the collision process and the bath gas density. If one assumes the collisional rate constant predicted by LGS theory,[1]

$$k = 2\pi e(\alpha/\mu)^{1/2}, \tag{12}$$

where $\mu = mM/(m+M)$ and $\alpha(N_2) = 1.74$ Å^3,[42] then the collision rate is 9.7×10^{-10} cm^3/s and O^+ undergoes between 200 and 350 collisions as it passes through the cell.

Besides translationally thermalizing the ions in the beam, these collisions remove the two metastable, electronically excited states of oxygen ion initially present, $O^+(^2D)$ and $O^+(^2P)$. The ^2D state has a radiative lifetime of 3.6 h and is removed via reaction (6) at a rate about 1/6 that given by Eq. (12).[34] The ^2P state has a radiative lifetime of 4.57 s and is removed via charge transfer with N_2, reaction (7), or the quenching process, reaction (8).[34] This latter process occurs at a rate about half the LGS limit, Eq. (12), while the rate for reaction (7) is an order of magnitude slower.[34] Ground state O^+ is also lost via reactions (2) and (5), but the efficiency of these processes is approximately 100 times less than that for removal of the excited state ions. The overall effect is thus a drastic reduction in the amount of excited state O^+ in the beam.

To determine the effectiveness of the state selection process, the charge transfer reaction of O^+ with N_2 is monitored in the main chamber as a function of kinetic energy. Since the ground state reaction, process (5), is endothermic by 1.96 eV, while the excited state reactions, processes (6) and (7), are exothermic, the presence of $O^+(^2D)$ or $O^+(^2P)$ in the beam can be easily detected by the formation of N_2^+ at low interaction energies. This is shown graphically in Fig. 2. As the pressure in the drift cell is increased, production of N_2^+ decreases. At drift cell pressures of 0.070 Torr or higher, low energy production of N_2^+ is no longer discernable from

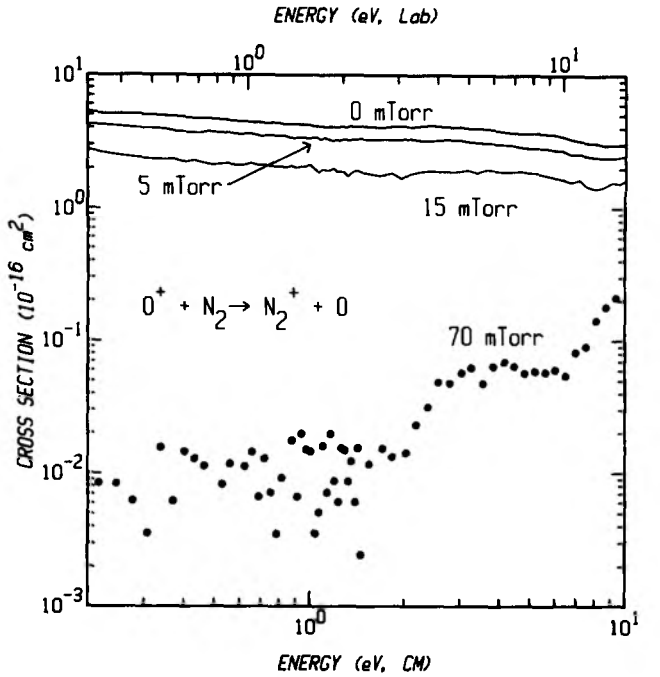

FIG. 2. Cross sections for the charge transfer reaction of O^+ with N_2 as a function of relative translational energy (lower scale) and laboratory energy (upper scale). The O^+ is generated by electron impact ionization of O_2 at 70 eV. Results are shown for four different nitrogen pressures in the drift cell.

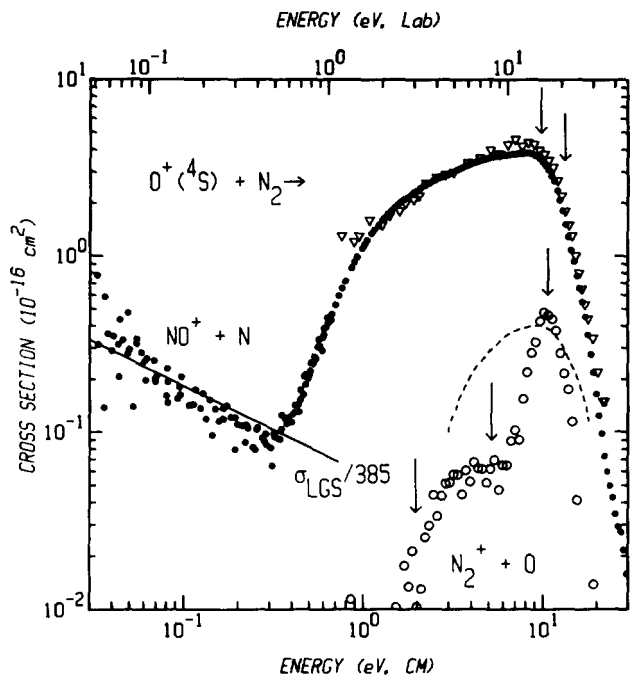

FIG. 3. Cross sections for reactions (2) (filled circles) and (5) (open circles) as a function of relative translational energy (lower scale) and laboratory energy (upper scale). The O^+ is generated by electron impact ionization of CO_2 at 70 eV and passed through the drift cell filled with N_2. For the $NO^+ + N$ channel, arrows indicate the thermodynamic and spectator stripping dissociation energies of NO^+ at 9.76 and 13.3 eV, respectively. For the $N_2^+ + O$ channel, arrows designate the thermodynamic thresholds for production of N_2^+ ($X\,^2\Sigma_g^+$) at 1.96 eV and of N_2^+ ($B\,^2\Sigma_u^+$) at 5.2 eV, and the thermodynamic dissociation energy of N_2^+ at 10.7 eV. Also included are cross section data from Ref. 5 for reaction (2) (open triangles), a phase space cross section for reaction (5) from Ref. 33 (dashed line), and the LGS cross section [Eq. (1)] scaled down by a factor of 385 (solid line).

random background noise, but above 2 eV the cross section for the reaction of $O^+(^4S)$ is clearly visible. For a beam initially consisting of 30% excited state (^2D and ^2P) ions, a *rigorous* upper limit of 0.06% can be placed on the total amount of excited state O^+ present after state selection at $P(N_2) = 70$ mTorr by assuming that the base line scatter at low energies results exclusively from reactions (6) and (7). To ensure that excited states are completely eliminated, the ion source conditions used in the rest of the report differ from those of Fig. 2 in two respects. First, drift cell pressures are maintained at 0.150 ± 0.010 Torr, more than twice the maximum shown in Fig. 2. This minimizes the effect of minor pressure fluctuations within the drift cell on the state selection process, and further insures that the excited state ions are completely removed. Second, CO_2 is used as the source gas so that fewer excited state ions are initially present.[6] Thus, the actual percentage of excited state ions in beams produced under these operating conditions is probably far below 0.06%.

RESULTS

Charge transfer reaction

The cross section for reaction (5), shown in Figs. 2 and 3, exhibits an onset near the thermodynamic threshold of 1.96 eV for production of ground state N_2^+ ($X\,^2\Sigma_g^+$). the cross section then rises in an interesting, double-humped fashion to give an early plateau and a secondary threshold near 6 eV. This second feature may be due to formation of N_2^+ ($B\,^2\Sigma_u^+$), which lies 3.2 eV above the ground state, and thus has a threshold at 5.2 eV. Finally, the cross section reaches a sharp maximum at about 10 eV before declining rapidly. This peak appears to correspond to dissociation of the N_2^+ product, which can begin at 10.7 eV.[43] However, the absolute cross sections for the charge transfer process may not be completely reliable, especially at higher energies, because of inefficient collection of the N_2^+ product. Charge transfer products are susceptible to losses since they can be formed with little forward velocity in the laboratory frame.

The overall magnitude of the present result is in good agreement with the phase space calculations of Wolf,[33] Fig. 3. The shape of the predicted cross section does not contain the sharp secondary threshold observed here but does show a decline beginning at about 10 eV. This decrease in the cross section prevents the present data from extrapolating smoothly to the results of Moran and Wilcox,[44] who measured a slowly increasing cross section of $\sim 10^{-16}$ cm^2 at laboratory energies above 500 eV, $E_0 > 318$ eV. This may simply be due to the differing energy regions examined but may also be caused by the inefficient collection mentioned above. In another study, Ottinger and Simonis[45] observed emission from N_2^+ ($B\,^2\Sigma_u^+$) product at a laboratory energy of 1000 eV, $E_0 = 636$ eV. The cross section measured for this

process was 4.6×10^{-18} cm^2. Again no direct comparison with the present results can be made.

Nitrogen atom abstraction: Cross sections

At interaction energies below 0.25 eV, the cross section for reaction (2) decreases as the energy is increased. The energy dependence of the decline is similar to the $E^{-0.5}$ dependence predicted by the LGS model, Eq. (1). The magnitude of the measured cross section, however, is approximately 400 times less than that predicted by Eq. (1). Between 0.25 and 2.0 eV, the cross section rises rapidly with increasing energy. At energies above 2.0 eV, the cross section rises more gently until a maximum of $\sim4.0\times10^{-16}$ cm^2 is observed near 8 eV. Shortly after this maximum, dissociation of the NO^+ product to $O^+(^4S)$ and $N(^4S)$ becomes energetically possible. The overall process,

$$O^+ + N_2 \rightarrow O^+ + N + N, \qquad (13)$$

has a thermodynamic threshold equal to $D^\circ(N_2) = 9.76$ eV.[43]

Also shown in Fig. 3 are the cross section results from Rutherford and Vroom.[5] Agreement between the two sets of data is excellent. Similar agreement is noted with an earlier experiment of Giese,[2] although his rather scattered data are not plotted here. Results of Stebbings, Turner, and Rutherford[10] also show approximate agreement with the current report, but cannot be compared directly because of a significant presence of excited state O^+ in their ion beam.

One interpretation of previous beam studies which deserves comment concerns the spectator stripping model (SSM).[46] Both the merged beam results of Neynaber and Magnuson[8] and Leventhal's[4] kinetic energy measurements indicate that the peak velocity of the NO^+ product in reaction (2) can be adequately represented by the SSM for the energy range $2 \leqslant E_0 \leqslant 12$ eV. However, the SSM also predicts that the NO^+ product becomes unstable with respect to dissociation at a kinetic energy given by

$$E_S = (D^\circ + \Delta H^\circ)\cdot(2m + M)/(m + M), \qquad (14)$$

where D° is the bond dissociation energy of NO^+ and ΔH° is the exothermicity of the reaction.[46] For reaction (2), the value of E_S, 13.3 eV, is marked by an arrow in Fig. 3. Clearly, the decline in the cross section for NO^+ correlates not with E_S but with the thermodynamic threshold at 9.8 eV. This shows that the *distribution* of product internal energies (and therefore, product kinetic energies as well) is not adequately described by the simplistic and physically unrealistic SSM.

Nitrogen atom abstraction: rate constants

It is of interest to compare directly the present cross section results with those of FA and FD experiments which measure reaction rates. To do this, the cross sections are converted into phenomenological rate constants using Eq. (15),

$$k(\langle E\rangle) = v_0\cdot\sigma(E_0), \qquad (15)$$

where $v_0 = (2E_0/\mu)^{1/2}$. The rate constants are a function of the mean relative energy of the reactants, $\langle E\rangle = E_0 + (3/2)\gamma k_B T$, where $\gamma = m/(m+M)$, k_B is Boltzmann's constant, and T is the temperature of the N_2 reactant gas (305 K). In the limit that $E_0 \rightarrow 0$, $k(\langle E\rangle)$ approaches the "bulk" thermal rate constant for the temperature $T' = \gamma\cdot T = 110$ K. Rate constants derived in this manner are directly comparable with those measured in FA and FD experiments once the differences in the ion energy distributions are taken into account.

Figure 4 presents the phenomenological rate constant $k(\langle E\rangle)$ for reaction (2), as calculated by Eq. (15). Also shown in Fig. 4 are the FA results of Ferguson *et al.*,[19] and the FD measurements of Albritton *et al.*[13] and Johnsen and Biondi.[11] Considering the very different methods used to obtain these results and the slowness of the reaction, the qualitative agreement is rather good. The general energy dependence is comparable and the absolute magnitudes of the rate constants are within a factor of 5 at all energies. Nevertheless, the quantitative comparison is somewhat disappointing since the observed differences lie outside the combined range of experimental error for the ion beam ($\pm$ 20%) and FD or FA experiments ($\pm$ 30%).

We have carefully eliminated several possible explanations for why our observed rate constants are higher at low energies. As noted above, the relative uncertainty of the measured cross sections (and rate constants) is less than 20% even at the lowest point. The absolute magnitudes shown here were reproduced several times during the course of several months of experimentation. The *maximum* contribution from excited state O^+ is calculated to be a factor of 5 less

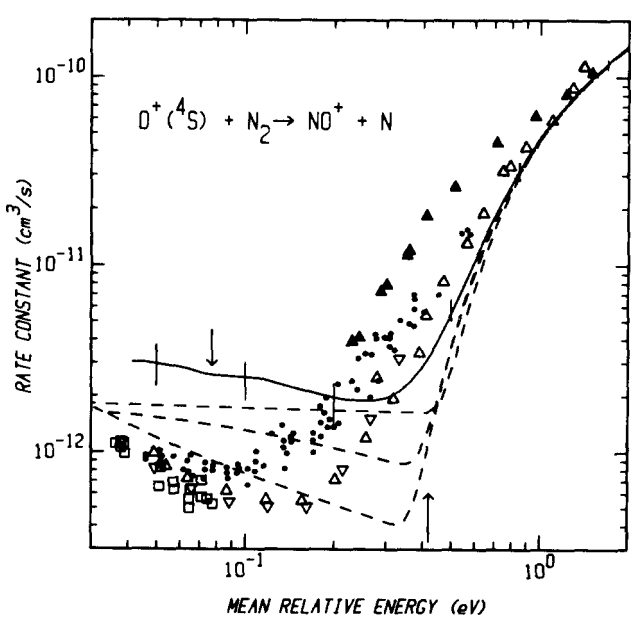

FIG. 4. Phenomenological rate constants for reaction (2) as a function of the mean relative energy of the reactants. The present data (solid line with error bars) are derived from the cross section data in Fig. 3 through the use of Eq. (15). Also included are the flowing afterglow results of Ref. 19, (open squares), the flow/drift tube results of Ref. 11 (solid circles), and the argon (solid triangles) and helium (open triangles) buffered FD data from Ref. 13. The upper, lower, and middle dashed lines correspond to the rate constants obtained from the unconvoluted forms of models I, II, and III, respectively, which are discussed in the text. Vertical arrows are located at 0.10 eV and 0.64 eV lab, the two energies examined in Fig. 7.

than the lowest cross section (or rate constant) measured. The possibility that the energy of the ions is influenced by the rf power driving the octopole was found to be negligible. The shape of the cross sections did not change with octopole power and the magnitudes were reproducible within 20% at all kinetic energies. Cross sections are independent of N_2 pressure throughout the energy range examined as expected for a single bimolecular event. We believe that the disagreements between the present data and the FD and FA data are caused primarily by differences in ion energy distributions. These differences are discussed in detail below.

DISCUSSION

While the experimentally measured cross sections and rate constants are reasonable approximations to the true cross sections and rate constants, the experimental conditions broaden sharp features in their behavior as a function of kinetic energy. In this section, we consider how the distribution of ion kinetic energies and the random thermal motion of the reactant gas obscure the true cross section. It is not possible to determine a unique form for the true cross section by directly deconvoluting the energy-broadened experimental results.[36] We therefore use an indirect method in which a particular model for the true cross section is convoluted over the experimental distributions of ion and neutral energies.[36,47] The convoluted form of the trial cross section is then compared directly to the experimentally observed cross section. Finally, the parameters of the trial function are adjusted to obtain the best possible fit to the actual data.

The simplest cross section model (which we will refer to as I) is completely empirical and uses the equation,

$$\sigma(E) = \sigma_1 E^{-u} + \sigma_2(1 - E_T/E)^w, \quad (16)$$

where σ_1, u, σ_2, E_T, and w are adjustable parameters. E is the *true* interaction energy between the reactants and differs from the energies E_0 and $\langle E \rangle$ which are average values for particular experimental distributions of energies. The first term in Eq. (16) accounts for the exothermic behavior at low energies and the second term accounts for the endothermic behavior at high energies. The specific form of Eq. (16) which is found to best represent the data corresponds to $\sigma_1 = 3.6 \pm 1.0 \times 10^{-18}$ cm^2 eV^u, $u = 0.53 \pm 0.10$, $\sigma_2 = 4.4 \pm 0.2 \times 10^{-16}$ cm^2, $E_T = 0.40 \pm 0.10$ eV, and $w = 2.8 \pm 0.8$. As shown in Fig. 5, convolution of this model over the experimental distribution of energies yields a result which is in excellent agreement with the present data at all energies. Also shown in Fig. 5 is a model for the decline in the cross section at energies above 9.76 eV. This model is described in detail in a previous report.[48,49]

A somewhat more sophisticated model, II, can be developed by incorporating Landau–Zener theory[50,51] to calculate the probability of a transition from the $1\,^4A''$ surface to the $1\,^2A''$ surface during the course of a collision. This probability[50–52] is

$$P = 2p(1-p), \quad (17)$$

where

$$p = \exp[-(A/E_C)^{1/2}] \quad (18)$$

is the probability of staying on the $1\,^4A''$ surface upon a single passage of the N_2O^+ system through the $1\,^4A''$–$1\,^2A''$ intersection, A^2 is the coupling strength between the two surfaces, and E_C is the relative kinetic energy at the intersection. Multiplication of the LGS collision cross section, σ_L as given by Eq. (1), by P gives the Landau–Zener cross sections for reaction (2) at energies below E_T. In the limit of small A, Eq. (17) and Eq. (18) simplify to $P = 2(A/E_C)^{1/2}$ such that

$$\sigma(E) = 2\sigma_L(A/E_C)^{1/2}, \quad E < E_T. \quad (19)$$

The overall form of the expression for the cross section is now

$$\sigma(E) = 2\sigma_L(A/E_C)^{1/2} + \sigma_2(1 - E_T/E)^w, \quad (20)$$

where the second term is unchanged from Eq. (16). This expression contains two new parameters, A and E_C. In the absence of any information regarding these quantities, a simple treatment assumes that $E_C = E$ and treats A as an adjustable parameter. The best fit between this model and the data is obtained when $A = 1.3 \times 10^{-8}$ eV, $\sigma_2 = 4.5 \pm 0.2 \times 10^{-16}$ cm^2, $E_T = 0.28 \pm 0.05$ eV, and $w = 4.3 \pm 0.9$. The unconvoluted form of this model has an E^{-1} energy dependence, which is appreciably steeper than the $E^{-0.53}$ dependence of the first model. Because of this, the convoluted form of the second model reaches a considerably smaller minimum that skirts the lower edge of the data in the region before threshold, Fig. 5.

A third model, III, uses Eq. (20) in conjunction with Hopper's calculated result[28] that the crossing between the $1\,^4A''$ and $1\,^2A''$ surfaces occurs at an energy 0.10 eV below

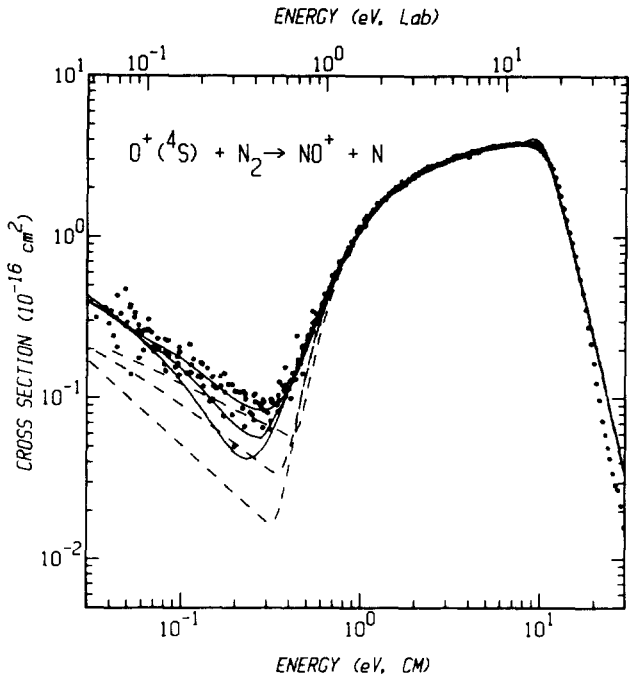

FIG. 5. Cross sections for reaction (2) as a function of the relative translational energy (lower scale) and laboratory energy (upper scale). The data (solid circles, same as Fig. 3) are compared with the three cross section models discussed in the text (dashed lines) and their convolutions over the experimental energy distribution (solid lines). Models I, II, and III correspond to the upper, lower, and middle curves, respectively.

that of the separated O^+ and N_2 reactants. Now, $E_C = E + 0.10$ eV and the energy dependence of the first term in Eq. (20) is intermediate to that of the first two models. The best fit to the data is obtained when $A = 8.3 \times 10^{-8}$ eV, $\sigma_2 = 4.5 \pm 0.2 \times 10^{-16}$ cm^2, $E_T = 0.30 \pm 0.06$ eV, and $w = 4.0 \pm 0.7$, Fig. 5.

The average value of E_T from all three models is 0.33 ± 0.08 eV. This lies within the 0.2–0.5 eV estimate of the "effective" adiabatic barrier calculated by Hopper.[32] Furthermore, the relative behavior of the present results compares favorably with Hopper's semiclassical trajectory calculations[32] using $E_T = 0.25$ and 0.99 eV, Fig. 6. This lends support to Hopper's conclusions concerning the topology of the $1\,^4A''$ hypersurface.

In contrast, the current results cannot be interpreted with the main mechanism hypothesized by Hopper[28] for energies below the adiabatic threshold, mechanism (3a, 3b, 3c). In the first step of this mechanism, reaction (3a) a three-body collisional stabilization occurs to trap N_2–$O^+(1\,^4A'')$ in a shallow potential energy well due to the ion-induced dipole attraction, Fig. 1. Given the improbability of secondary ion-molecule collisions within the interaction region of our apparatus, such a mechanism can be ruled out for the formation of NO^+ observed in this study. In addition, the ability of Landau–Zener theory[50–52] to account for the low energy cross section results confirms the feasibility of mechanism (4), the single collision, spin-forbidden process.

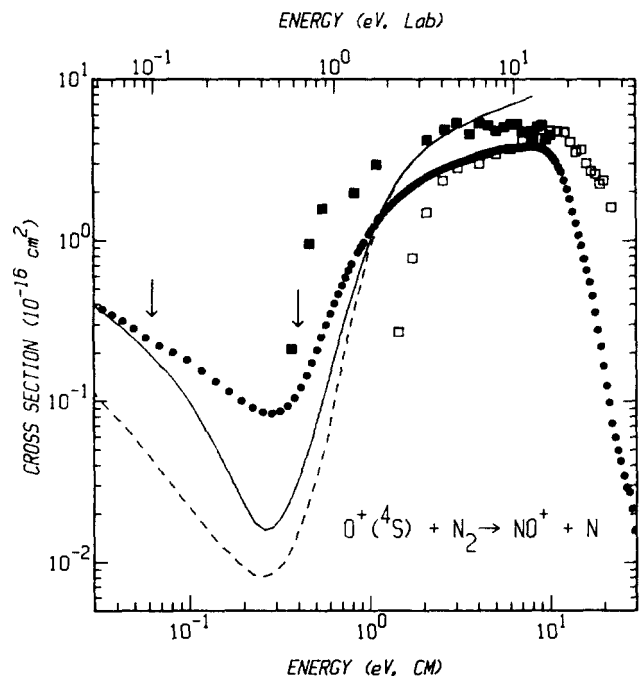

FIG. 6. Cross sections for reaction (2) as a function of the relative translational energy (lower scale) and laboratory energy (upper scale). The present results are given by the solid circles and represent an average of the data shown in Fig. 3. The cross section derived by Albritton and coworkers (Ref. 13) and its convolution over the distribution of energies in the present ion beam experiment are designated by the dashed and solid lines, respectively. Results of Hopper's semiclassical trajectory calculations (Ref. 32) are denoted by the solid (0.25 eV barrier height) and open (0.99 eV barrier height) squares. Vertical arrows are located at 0.10 eV and 0.64 eV lab, the two energies examined in Fig. 7.

This is particularly evident from a comparison of the values of A found here (10^{-7}–10^{-8} eV) to the value of 2.7×10^{-5} eV estimated by Tully[53] for a similar system, the spin-forbidden unimolecular decomposition of nitrous oxide to $N_2(^1\Sigma_g^+)$ and $O(^3P)$. Since the values of A which fit the present data are *smaller* than this, it is clear that the present agreement with a Landau–Zener model does not require an unreasonably large coupling constant.

Also shown in Fig. 6 is the cross section derived from the FD data of Albritton *et al.*[13] This result was obtained using a procedure similar to our own. Specifically, a trial cross section is convoluted with ion and neutral energy distributions and compared with FD rate constant data in both He and Ar buffers. The shape of the cross section is adjusted until both sets of data are reproduced. The difference between this procedure and ours is that we are able to measure the ion energy distribution directly, while this is calculated[54,55] for the FD work. This calculation involves two steps. First, an ion–neutral interaction potential is derived from a series of ion mobility measurements.[56,57] Then, the derived potential is used to estimate the ion energy distribution corresponding to a particular set of experimental conditions. Figure 6 makes it clear that a substantial disagreement exists *at all energies* between the present results and the cross section derived from the FD data. This is despite the fact that the FD data and the present results converted to rate constants agree at elevated energies, Fig. 4. In general, this demonstrates how very difficult it is to convert from a macroscopic rate constant to a microscopic cross section.

A qualitative understanding of the origins of the disagreement can be gleaned from an examination of the ion energy distributions associated with each experiment. In both the FD and the ion beam studies, the N_2 reactant has a thermal distribution of energies corresponding to the ambient temperature, ~300 K. In the present beam experiment, the incident $O^+(^4S)$ ions have a Gaussian energy distribution with a FWHM of 0.2 eV (0.3 eV lab). This energy distribution does not change with kinetic energy until truncation of the slow ions which occurs at energies less than ~0.2 eV. In the FD (and FA) rate constant determinations, the presence of a high pressure buffer gas (He or Ar) insures that the ions maintain a Maxwellian distribution at low energies. In the FD experiments, the ions are accelerated through the buffer gas by a weak electric field. As the field strength increases, the distribution of ion energies begins to deviate from a Maxwellian distribution in a manner which depends on the detailed interactions of the ion with the buffer gas. Since accurate experimental determinations of the true distribution of reactant energies have not yet proven possible, it is necessary to estimate (or calculate) the distributions as outlined above.[13]

Figure 7(a) compares the ion speed distributions for these experiments at an average laboratory energy of 0.64 eV ($E_0 = 0.41$ eV, $\langle E \rangle = 0.42$ eV).[58] It can be seen that the distribution for the ion beam is by far the narrowest. Distributions in He and Ar buffers are similar to Maxwell–Boltzmann (MB), but the He distribution has fewer high speed ions than the Ar distribution. As one progresses from beam to He buffer to Ar buffer, there are more kinetically "hot"

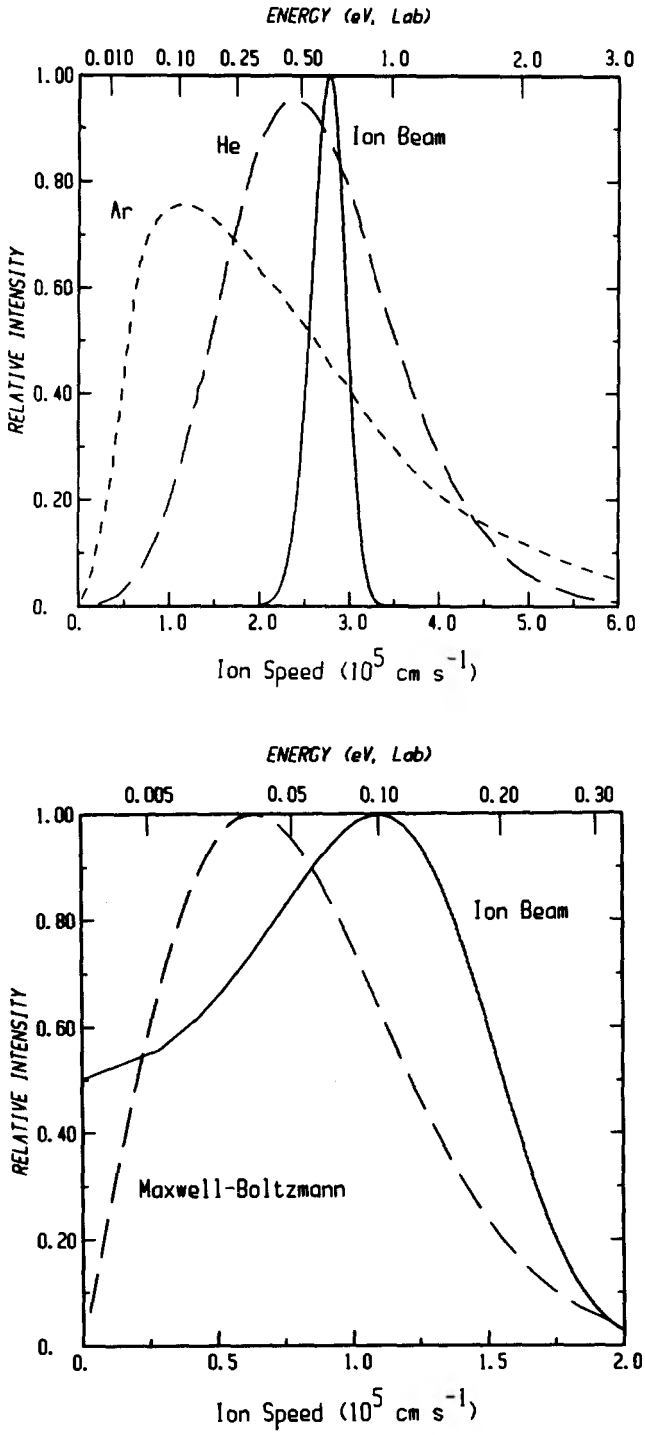

FIG. 7. Ion speed (lower scale) and energy (upper scale) distributions for an average laboratory energy of 0.64 eV (part a) and 0.10 eV (part b). The distributions from the present experiment are shown by the solid lines, and the FD distributions (Ref. 58) are shown by the dashed (Ar buffer) and broken (He buffer) lines. The Maxwell–Boltzmann distribution is given by a broken line in part b.

ions with speeds that correspond to larger cross sections. Thus, the apparent threshold for reaction (2) is lower in the Ar buffer than in the He buffer which in turn is lower than in the beam data which in turn is lower than the true threshold energy, $E_T \approx 0.3$ eV. This progression is easily seen in Fig. 4.

The discrepancy between our "true" cross section and the FD cross section above ~ 0.3 eV is now clear. In the threshold region, the FD cross section is smaller than the beam cross section while at higher energies the FD cross section is larger, Fig. 6. These differences in cross section magnitude probably compensate for one another during the convolution over the FD ion energy distributions, which are quite broad at these energies. In contrast, the experimental energy distributions in the ion beam experiment are much narrower at elevated energies. This is clearly demonstrated by the fact that, above 0.7 eV, the measured and true cross sections do not differ appreciably, Fig. 5.

The situation at low interaction energies is qualitatively different. This is shown in Fig. 7(b), which compares the ion beam speed distribution at a laboratory energy of 0.10 eV ($E_0 = 0.064$ eV, $\langle E \rangle = 0.078$ eV) to a MB distribution having the same average energy, $3k_B T/2$ ($T = 774$ K). The MB distribution exactly reproduces the speed distribution in FA studies and is a reasonable approximation to the distribution found in FD experiment. At this energy, the FA and FD distributions are narrower and have a lower most-probable speed than the ion beam distribution. The high pressure conditions of the FA and FD experiments now serve to reduce the spread of the reactant energies compared to the static FWHM of the ion beam. Just as energy broadening in the FD experiment gave results which were high in the region near threshold, energy broadening in the beam experiment produces high results at low energies. One factor in particular plays an important role in this process. At low energies, slow ions are truncated from the ion beam distribution. This shifts the peak of the ion speed distribution towards zero and yields more ions with very low velocities than a MB distribution. Since ions with speeds near zero correspond to very large cross sections, this causes the ion beam method to give high cross section results at very low energies.

The effect can be seen both in Fig. 6 and Fig. 4. Figure 6 shows that convolution of the FD derived cross section[13] over the present experimental distribution of energies yields a result which is in agreement with the present data at the lowest energies. Figure 4 shows that model II [Eq. (20) with $E_C = E$] converts to a rate constant which matches the FA and FD data within experimental uncertainties. Because this model is roughly consistent with all sets of data it is probably the best estimate of the true cross section over the energy range examined.

Unfortunately, differences in ion energy distributions do not appear to account for the disagreements observed immediately before the adiabatic threshold, from about 0.1 to 0.3 eV. This discrepancy is probably a reflection of the joint experimental uncertainties involved in measurements of very slow reactions at these energies; however, it is possible that some of the residual discrepancy results from differences in interaction region pressure. This is the other major difference in experimental conditions between the ion beam and the FA and FD studies besides the energy distributions. The differences between the present data and the FA and FD rate constant data imply that three-body collisional stabilization diminishes production of NO^+ at low interaction energies. However, Bohme *et al.*[23] have found the opposite ef-

fect and shown that the reaction rate increases with increasing He buffer gas pressure at 82 K, $\langle E \rangle = 0.011$ eV. This study may not be definitive, however, since the rate constant was obtained by measuring the decline in the O^+ signal. In their detailed study of this system, Albritton *et al.*[13] concluded that erroneous rate constants are obtained for this reaction when measured in this manner. Further FD measurements on the quantitative three-body pressure dependence of reaction (2) at low energies would help to resolve this issue.

The observation that the reaction rate increases with increasing buffer gas pressure[23] supports Hopper's predictions[28] that collisional stabilization of N_2O^+ promotes reaction at low energies, reaction scheme (3). At the same time, both the present results and Landau–Zener[50–52] theory indicate that reaction can occur via a single collision process, reaction scheme (4). Together, these observations imply that at low pressures reaction (2) proceeds via a single collision process, and at higher pressures, reaction may be enhanced via process (3). At energies above threshold, where the reactants are not required to undergo a spin-forbidden transition, this pressure dependence is not expected to play a major role.

CONCLUSION

Guided ion beam mass spectrometry has been used to examine the kinetic energy dependence of the reaction of ground state atomic oxygen ion with molecular nitrogen from 0.03 to 30 eV. This represents a much wider energy range than has been examined previously in any single ion beam, flowing afterglow (FA), or flow/drift (FD) study. Cross sections for the $NO^+ + N$ product channel show an exothermic dependence on kinetic energy below 0.25 eV. The present results demonstrate that this reactivity occurs via single collision mechanism, Eq. (4), which can be modeled using a Landau–Zener formalism. At higher energies, the cross sections exhibit an endothermic kinetic energy dependence with an apparent threshold of 0.33 ± 0.08 eV. This corresponds to the effective activation barrier on the quartet reaction surface.

The present results are in good qualitative agreement with all previous beam, FA, and FD studies. This demonstrates that the guided ion beam technique can provide reasonably accurate experimental cross sections and rate constants throughout the energy range examined. However, the present data (converted to rate constant form) and the results of FA and FD studies do not agree quantitatively. The disagreements are shown to result primarily from differences in ion energy distributions. A model, II, for the true cross section behavior which is consistent within experimental error with the FA, FD, and beam data is derived. Our model differs from the true cross section previously derived from FD data. This latter cross section is inconsistent with the cross sections measured directly in the present experiment. The discrepancy is almost certainly due to the extreme difficulties in accounting for the distribution of ion energies in FD studies. Finally, we point out that differences in interaction region pressures between the FA and FD studies and the ion beam study could also influence the reaction rate observed at low energies. Additional work would be useful in uncovering the low energy dynamics associated with reaction (2) and in ascertaining the role of multiple collisions in this process.

ACKNOWLEDGMENTS

This work is supported by NSF Grant No. CHE-8608847. We thank E. E. Ferguson for helpful comments.

[1] G. Gioumousis and D. P. Stevenson, J. Chem. Phys. **29**, 294 (1958).
[2] C. Giese, in *Ion–Molecule Reactions in the Gas Phase*, edited by P. J. Ausloos (American Chemical Society, Washington, D.C., 1966), p. 20.
[3] B. R. Turner, J. A. Rutherford, and D. M. J. Compton, J. Chem. Phys. **48**, 1602 (1968).
[4] J. J. Leventhal, J. Chem. Phys. **54**, 5102 (1971).
[5] J. A. Rutherford and D. A. Vroom, J. Chem. Phys. **55**, 5622 (1971).
[6] B. M. Hughes and T. O. Tiernan, J. Chem. Phys. **55**, 3419 (1971).
[7] R. B. Cohen, J. Chem. Phys. **57**, 676 (1972).
[8] R. H. Neynaber and G. D. Magnuson, J. Chem. Phys. **58**, 4586 (1973).
[9] G. P. K. Smith and R. J. Cross, Jr., J. Chem. Phys. **60**, 2125 (1974).
[10] R. F. Stebbings, B. R. Turner, and J. A. Rutherford, J. Geophys. Res. **71**, 771 (1966).
[11] R. Johnsen and M. A. Biondi, J. Chem. Phys. **59**, 3504 (1973).
[12] M. McFarland, D. L. Albritton, F. C. Fehsenfeld, E. E. Ferguson, and A. L. Schmeltekopf, J. Chem. Phys. **59**, 6620 (1973).
[13] D. L. Albritton, I. Dotan, W. Lindinger, M. McFarland, J. Tellinghuisen, and F. C. Fehsenfeld, J. Chem. Phys. **66**, 410 (1977).
[14] R. Johnsen and M. A. Biondi, J. Chem. Phys. **73**, 190 (1980).
[15] D. Smith, N. G. Adams, and T. M. Miller, J. Chem. Phys. **69**, 308 (1978).
[16] J. Glosik, A. B. Rakshitt, N. D. Twiddy, N. G. Adams, and D. Smith, J. Phys. B **11**, 3365 (1978).
[17] A. L. Schmeltekopf, E. E. Ferguson, and F. C. Fehsenfeld, J. Chem. Phys. **48**, 2966 (1968).
[18] D. B. Dunkin, F. C. Fehsenfeld, A. L. Schmeltekopf, and E. E. Ferguson, J. Chem. Phys. **49**, 1365 (1968).
[19] E. E. Ferguson, D. K. Bohme, F. C. Fehsenfeld, and D. B. Dunkin, J. Chem. Phys. **50**, 5039 (1969).
[20] D. K. Bohme, D. B. Dunkin, F. C. Fehsenfeld, and E. E. Ferguson, J. Chem. Phys. **49**, 5201 (1968).
[21] G. F. O. Langstroth and J. B. Hasted, Discuss. Faraday Soc. **33**, 298 (1962).
[22] J. Sayers and D. Smith, Discuss. Faraday Soc. **37**, 167 (1964).
[23] D. K. Bohme, D. B. Dunkin, F. C. Fehsenfeld, and E. E. Ferguson, J. Chem. Phys. **51**, 863 (1969).
[24] J. J. Kaufman and W. S. Koski, J. Chem. Phys. **50**, 1942 (1969).
[25] T. F. O'Malley, J. Chem. Phys. **52**, 3269 (1970).
[26] A. Pipano and J. J. Kaufman, J. Chem. Phys. **56**, 5258 (1972).
[27] D. G. Hopper, Chem. Phys. Lett. **31**, 446 (1975).
[28] D. G. Hopper, J. Am. Chem. Soc. **100**, 1019 (1978).
[29] D. G. Hopper, J. Chem. Phys. **72**, 3679 (1980).
[30] D. G. Hopper, J. Chem. Phys. **72**, 4676 (1980).
[31] D. G. Hopper, J. Chem. Phys. **76**, 1068 (1982).
[32] D. G. Hopper, J. Chem. Phys. **77**, 314 (1982).
[33] F. A. Wolf, J. Chem. Phys. **44**, 1619 (1966).
[34] E. E. Ferguson, F. C. Fehsenfeld, and D. L. Albritton, in *Gas Phase Ion Chemistry*, edited by M. T. Bowers (Academic, New York, 1979), Vol. 1, p. 53.
[35] Although Rutherford and Vroom (Ref. 5) limit their discussion to the inability of $O^+(^2D)$ to produce NO^+, their analysis is equally valid for $O^+(^2P)$. Given the efficiency at which $O^+(^2P)$ is collisionally quenched to $O^+(^4S)$, reaction (8), appreciable formation of NO^+ from $O^+(^2P)$ is highly unlikely.
[36] K. M. Ervin and P. B. Armentrout, J. Chem. Phys. **83**, 166 (1985).
[37] N. R. Daly, Rev. Sci. Instrum. **31**, 264 (1960).
[38] At the low pressures of the present study, the probability of the jth order collision is given by $(n \cdot l \cdot \sigma_L)^j$, where n is the number density of the N_2 and l is the length of the interaction region (8.6 cm).
[39] P. A. M. Van Koppen, P. R. Kemper, A. J. Illies, and M. T. Bowers, Int. J. Mass Spectrom. Ion Proc. **54**, 263 (1983).

[40]K. M. Ervin and P. B. Armentrout, J. Chem. Phys. **84**, 6738 (1986).
[41]E. W. McDaniel and E. A. Mason, *The Mobility and Diffusion of Ions in Gases,* (Wiley, New York, 1973), Table 7-1-H-1.
[42]E. W. Rothe and R. B. Bernstein, J. Chem. Phys. **31**, 1619 (1959).
[43]K. P. Huber and G. Herzberg, *Constants of Diatomic Molecules,* (Van Nostrand Reinhold, New York, 1979).
[44]T. F. Moran and J. B. Wilcox, J. Chem. Phys. **69**, 1397 (1978).
[45]C. Ottinger and J. Simonis, Chem. Phys. **28**, 97 (1978).
[46]A. Henglein and K. Lacmann, Adv. Mass. Spectrom. **3**, 331 (1966); A. Henglein, in *Ion–Molecule Reactions in the Gas Phase,* edited by P. J. Ausloos (American Chemical Society, Washington, D. C., 1966), p. 63; A. Ding, K. Lacmann, and A. Henglein, Ber. Bunsenges. Phys. Chem. **71**, 596 (1967).
[47]C. Lifshitz, R. L. C. Wu, T. O. Tiernan and D. T. Terwillger, J. Chem. Phys. **68**, 247 (1978).
[48]M. E. Weber, J. L. Elkind, and P. B. Armentrout, J. Chem. Phys. **84**, 1521 (1986).
[49]The best fit between the present cross section data and the fall-off model presented in Ref. 48 corresponds to $D = 9.76$ eV, $f = 1.0$, and $p = 4.0$.
[50]L. D. Landau, Phys. Z. Sowjetunion **2**, 46 (1932).
[51]C. Zener, Proc. R. Soc. London Ser. A **137**, 696 (1932).
[52]A. P. M. Baede, Ad. Chem. Phys. **30**, 463 (1975).
[53]J. Tully, J. Chem. Phys. **61**, 61 (1974).
[54]L. A. Viehland and E. A. Mason, J. Chem. Phys. **66**, 422 (1977).
[55]S. L. Lin and J. N. Bardsley, J. Chem. Phys. **66**, 435 (1977).
[56]W. Lindinger and D. L. Albritton, J. Chem. Phys. **62**, 3517 (1975).
[57]I. Dotan, W. Lindinger, and D. L. Albritton, J. Chem. Phys. **64**, 4544 (1976).
[58]D. L. Albritton, in *Kinetics of Ion—Molecule Reactions,* edited by P. J. Ausloos (Plenum, New York, 1979), p. 132.